Article
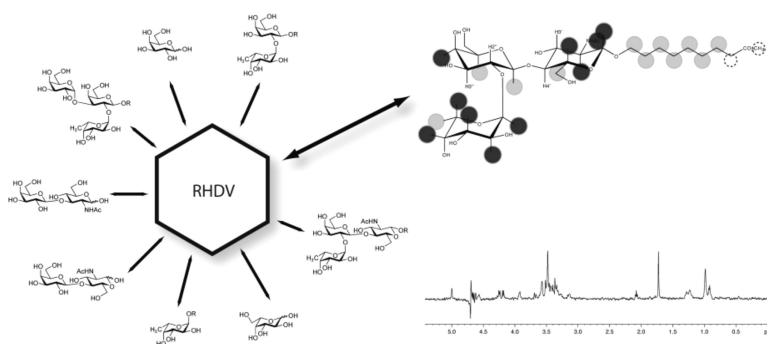
NMR Experiments Reveal the Molecular Basis of Receptor Recognition by a Calicivirus

Christoph Rademacher, N. Rama Krishna, Monica Palcic, Francisco Parra, and Thomas Peters

More About This Article

Additional resources and features associated with this article are available within the HTML version:

- Supporting Information
- Links to the 2 articles that cite this article, as of the time of this article download
- Access to high resolution figures
- Links to articles and content related to this article
- Copyright permission to reproduce figures and/or text from this article

View the Full Text HTML

NMR Experiments Reveal the Molecular Basis of Receptor Recognition by a Calicivirus

Christoph Rademacher,[†] N. Rama Krishna,[‡] Monica Palcic,[§] Francisco Parra,[∥] and Thomas Peters*,[†]

University of Luebeck, Institute of Chemistry, Ratzeburger Allee 160, 23538 Luebeck, Germany, University of Alabama at Birmingham, Birmingham, Alabama 35294-2041, Carlsberg Laboratory, Gamle Carlsberg Vej10, DK-2500 Valby, Denmark, and Instituto Universitario de Biotecnología de Asturias, Departamento de Bioquímica y Biología Molecular, Edificio Santiago Gascón, Campus El Cristo, Universidad de Oviedo, 33006 Oviedo, Spain

Received December 5, 2007; E-mail: thomas.peters@chemie.uni-luebeck.de

Abstract: The analysis of virus−receptor interactions at atomic resolution is of fundamental importance to understand infection processes, and to establish novel anti-viral therapies. As an example, rabbit hemorrhagic disease virus (RHDV), a member of the *Caliciviridae* family and considered as an "emerging" virus, attaches to histo-blood group antigens (HBGA) on the surface of adult rabbit epithelial cells of the upper respiratory and digestive tracts. It appears that this attachment is a key step in the process of infection with RHDV. Here, we report NMR experiments that reveal the atomic details of the recognition of HBGAs and fragments thereof by RHDV virus-like particles (VLP). The experiments yield binding epitopes of several HBGAs and show that L-fucose is a minimal structural requirement for specific molecular recognition by the VLPs. As the methodology is general, these studies may pave the way for the development of novel anti-viral entry inhibitors.

The family of *Caliciviridae* consists of four genera, *Norovirus*, *Sapovirus*, *Lagovirus*, and *Vesivirus*. With the exception of some *Vesiviruses* that can cause sporadic infections in humans, only members of the first two genera infect humans and usually cause gastroenteritis. RHDV is a member of the genus *Lagovirus* and infects rabbits leading to a severe hepatitis and death usually within 48 h. All *Caliciviridae* are non-enveloped viruses with positive strand RNA that is coated by self-assembling capsid proteins. Antigenicity and receptor specificity is dictated by the capsid. In two cases, for the *Norwalk virus* and the *San Miguel sea lion virus*, crystal structures of the complete capsid have been obtained.[1−3] Despite a rather low sequence similarity, the gross icosaedric shape of the virus capsid is very similar, and it is currently believed that the overall 3D structures of all members of the *Caliciviridae* family are rather alike. Therefore, the specific usage of receptors is due to fine details on the viral surfaces, that is, the binding pockets. Understanding receptor specificities at an atomic level is the basis for the development of so-called entry-inhibitors that may be used in prevention and therapy of viral infections.

Obviously, new approaches for the analysis of receptor−virus interactions at atomic level are of considerable interest. We have shown that saturation transfer difference (STD) NMR experiments are very powerful to detect and characterize the binding of small molecules to native human rhinoviruses,[4] and others have applied this methodology to, for example, whole cells.[5,6]

Here, we demonstrate that this methodology can be applied to map at atomic resolution the binding of receptor fragments to rabbit hemorrhagic disease virus (RHDV), a member of the *Caliciviridae* family.[7,8] Considering the lack of hemorrhagic disease reports before the first outbreaks described in 1984 in China,[9] RHDV can be regarded as an emerging virus, possibly derived from a non-pathogenic ancestor.

For RHDV, no structural information from X-ray crystallography is available that makes RHDV a challenging target. It is known that RHDV attaches to histo-blood group antigens (HBGAs) exposed on the surface of the host cell and that binding to this kind of antigens explains the different susceptibility of adult and young rabbits to RHDV.[10] It is also known

[†] University of Luebeck.
[‡] University of Alabama at Birmingham.
[§] Carlsberg Laboratory.
[∥] Instituto Universitario de Biotecnología de Asturias.

(1) Prasad, B. V.; Hardy, M. E.; Dokland, T.; Bella, J.; Rossmann, M. G.; Estes, M. K. *Science* **1999**, *286*, 287−90.
(2) Chen, R.; Neill, J. D.; Prasad, B. V. *J. Struct. Biol.* **2003**, *141*, 143−8.
(3) Chen, R.; Neill, J. D.; Estes, M. K.; Prasad, B. V. *Proc. Natl. Acad. Sci. U.S.A.* **2006**, *103*, 8048−53.

(4) Benie, A. J.; Moser, R.; Baeuml, E.; Blaas, D.; Peters, T. *J. Am. Chem. Soc.* **2003**, *125*, 14−5.
(5) Claasen, B.; Axmann, M.; Meinecke, R.; Meyer, B. *J. Am. Chem. Soc.* **2005**, *127*, 916−9.
(6) Mari, S.; Serrano-Gomez, D.; Canada, F. J.; Corbi, A. L.; Jimenez-Barbero, J. *Angew. Chem., Int. Ed.* **2004**, *44*, 296−8.
(7) Thiel, H. J.; Konig, M. *Vet. Microbiol.* **1999**, *69*, 55−62.
(8) Parra, F.; Prieto, J. M. *J. Virol.* **1990**, *64*, 4013−4015.
(9) Moss, S. R.; Turner, S. L.; Trout, R. C.; White, P. J.; Hudson, P. J.; Desai, A.; Armesto, M.; Forrester, N. L.; Gould, E. A. *J. Gen. Virol.* **2002**, *83*, 2461−7.
(10) Ruvoen-Clouet, N.; Ganiere, J. P.; Andre-Fontaine, G.; Blanchard, D.; Le Pendu, J. *J. Virol.* **2000**, *74*, 11950−4.

Scheme 1. ◇ Represents D-Galactose, ■ Represents
β-D-*N*-Acetyl-glucosamine, and △ Represents α-L-Fucose[a]
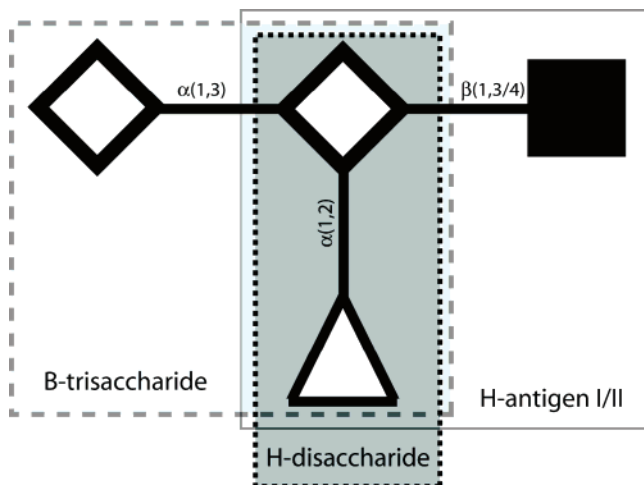
[a] The spatial presentation of the H-disaccharide or the B-trisaccharide depends on the type of glycosidic linkage between β-D-galactose and β-D-*N*-acetyl-glucosamine (type I or II).

that RHDV specifically binds to H-antigen type II structures[10] but not to type I structures. On the other hand, the prototype Norwalk virus that infects humans attaches to H-antigen type I structures but not to type II structures[11,12] (Scheme 1). Other Noroviruses display yet different blood group specificities.[13] In the following, we demonstrate that this exquisite receptor specificity can be mapped at atomic resolution using synthetic fragments (Scheme 2) of the blood group antigen receptors, without the need to analyze the 3D structure of RHDV.

Materials and Methods

Synthesis. Compound **1** was enzymatically synthesized.[14] Compound **2** was chemically synthesized (unpublished data). Compounds **3** and **4** were gifts from Prof. O. Hindsgaul, Carlsberg Laboratory. Compound **5** was obtained from Dextra, and compounds **6**−**9** were obtained from Sigma.

Expression and Purification of RHDV VLPS. To produce VP60, the major RHDV capsid component, the coding region from isolate AST-89 was directionally cloned into the baculovirus transfer vector pTriEx-SfiI[15] using *Nco*I and *Pst*I restriction sites. The pTriEx-VP60 construct was confirmed by nucleotide sequencing and *Escherichia coli* expression. The recombinant baculovirus Bac-Tri-VP60RHD was created using the pTriEx-VP60 transfer vector and the linearized modified bacmid DNA described by Zhao et al.[16] following a shortened protocol of Pengelley et al.[15] Baculovirus expressed recombinant VP60 was produced after infection of suspension Sf9 cultures with recombinant baculovirus Bac-Tri-VP60RHD at a multiplicity of infection of 5. The infected cultures were grown in Insect-XPRESS protein-free medium for 5 days at 28 °C, and the cells were harvested by centrifugation at 500*g* for 5 min. The culture supernatant was further clarified by centrifugation at 16 000 rpm for 20 min at 4 °C using a Kontron A8.24 rotor. RHDV VLPs in the above clarified culture supernatant were finally harvested and concentrated by ultracentrifu-

gation at 26.000 rpm for 150 min at 4 °C. The resulting sediment containing purified VLPs was suspended in 20 mM phosphate buffer pH 7.3, 130 mM NaCl.

NMR Sample Preparation. Buffer was exchanged three times using Microcon (100 kDa cutoff, Millipore) against 20 mM phosphate buffer pH 7.3, 130 mM NaCl, in D_2O at 4 °C utilizing an Eppendorf 5415D centrifuge. Centrifugations were performed at 13 000 rcf. The concentration of VLPs was 1.5−2.5 mg/mL (0.14−0.23 μM). Assuming the presence of 90 binding sites for each capsid, the concentration of binding sites was estimated to lie between 12 and 22 μM in a NMR sample.

Dynamic Light Scattering. Prior to NMR experiments, the homogeneity and intact capsid conditions were determined using dynamic light scattering. A Laser Spectroscatter (Rina GmbH) was utilized for this purpose at 689.8 nm wavelength at room temperature and a static angle of 90°. Forty independent measurements were averaged. The measurements did not give any indication of aggregation of VLPs.

NMR Experiments for Assignments. Carbohydrates were dissolved in D_2O at a concentration of 5 mM in D_2O. Assignments were done using standard two-dimensional NMR techniques in combination with one-dimensional gradient enhanced chemical shift selective filter experiments.[17] NMR experiments for the assignment were performed at 282 K. All spectra were recorded on a Bruker Avance 500 MHz NMR spectrometer equipped with a cryogenic probe. Bruker xwinnmr 3.5 and Topspin 1.3 were used for processing and analysis of one-dimensional spectra. For processing of two-dimensional spectra, nmrPipe was used.[18] These spectra were analyzed in CCPN.[19]

STD NMR. STD NMR spectra were recorded with a final concentration of VLPs of 0.14−0.23 μM (12−22 μM binding sites). Ligand concentrations ranged between 0.5 and 5 mM. A pseudo2D version of the STD NMR sequence was used to achieve interleaved acquisition of on- and off-resonance spectra. A 3-9-19 watergate sequence was used for water suppression. For saturation, a cascade of Gaussian pulses with a length of 49 ms and an attenuation of 50 dB were employed. The inter-pulse delay was 1 ms. Saturation times to record the buildup of STD effects were 0.35, 0.50, 0.75, 1.00, and 2.00 s if not stated otherwise. For epitope mapping, the on-resonance frequency was set at −4 ppm, and the off-resonance was set at 300 ppm. A relaxation delay of 25 s was used in all cases.[20] All spectra were recorded at 282 K. The number of scans was adjusted to the requirements of the specific samples and ranged between 128 and 3 K scans.

Variation of the Off-Resonance Frequency. STD NMR experiments with 128 scans for on- and off-resonance, respectively, were recorded utilizing 3-9-19 watergate for water suppression. The relaxation delay was 25 s not including the acquisition time of 2.73 s. The on-resonance frequency was kept constant at −4 ppm, while the off-resonance frequency was varied from −300 to +300 ppm. These experiments were repeated without water suppression leading to the same results apart from a lower S/N ratio (see Supporting Information). Data were fitted to a Lorenzian line shape (eq 1) using nonlinear least-square fitting as implemented in Scientific Python (http://www.scipy.org).

$$I(x) = I_0 - I_1\left(\frac{R}{R^2 + 4\pi^2(x-a)^2}\right) \qquad (1)$$

with $I(x)$ being the intensity measured as a function of the offset from the on-resonance condition ($x = a$), I_0 and I_1 being scaling factors, R

(11) Huang, P.; Farkas, T.; Zhong, W.; Tan, M.; Thornton, S.; Morrow, A. L.; Jiang, X. *Virology* **2005**, *79*, 6714−22.
(12) Harrington, P. R.; Vinje, J.; Moe, C. L.; Baric, R. S. *J. Virol.* **2004**, *78*, 3035−45.
(13) Tan, M.; Jiang, X. *Trends Microbiol.* **2005**, *13*, 285−93.
(14) Seto, N. O. L.; Compston, C. A.; Szpacenko, A.; Palcic, M. M. *Carbohydr. Res.* **2000**, *324*, 161−169.
(15) Pengelley, S. C.; Chapman, D. C.; Mark Abbott, W.; Lin, H. H.; Huang, W.; Dalton, K.; Jones, I. M. *Protein Expression Purif.* **2006**, *48*, 173−81.
(16) Zhao, Y.; Chapman, D. A.; Jones, I. M. *Nucleic Acids Res.* **2003**, *31*, E6−6.

(17) Robinson, P. T.; Pham, T. N.; Uhrin, D. *J. Magn. Reson.* **2004**, *170*, 97−103.
(18) Delaglio, F.; Grzesiek, S.; Vuister, G. W.; Zhu, G.; Pfeifer, J.; Bax, A. *J. Biomol. NMR* **1995**, *6*, 277−293.
(19) Vranken, W. F.; Boucher, W.; Stevens, T. J.; Fogh, R. H.; Pajon, A.; Llinas, M.; Ulrich, E. L.; Markley, J. L.; Ionides, J.; Laue, E. D. *Proteins* **2005**, *59*, 687−96.
(20) Rademacher, C.; Peters, T. *Top. Curr. Chem.* **2008**, *273*, in press.

Scheme 2. Carbohydrate Ligands Investigated: **1**, **3** R = (CH$_2$)$_7$CH$_3$; **2** R = ^{13}CH$_3$; **7** R = CH$_3$; **4** R = (CH$_2$)$_8$COOMe

1 **2**

3 **4**

5 **6**

7 **8** **9**
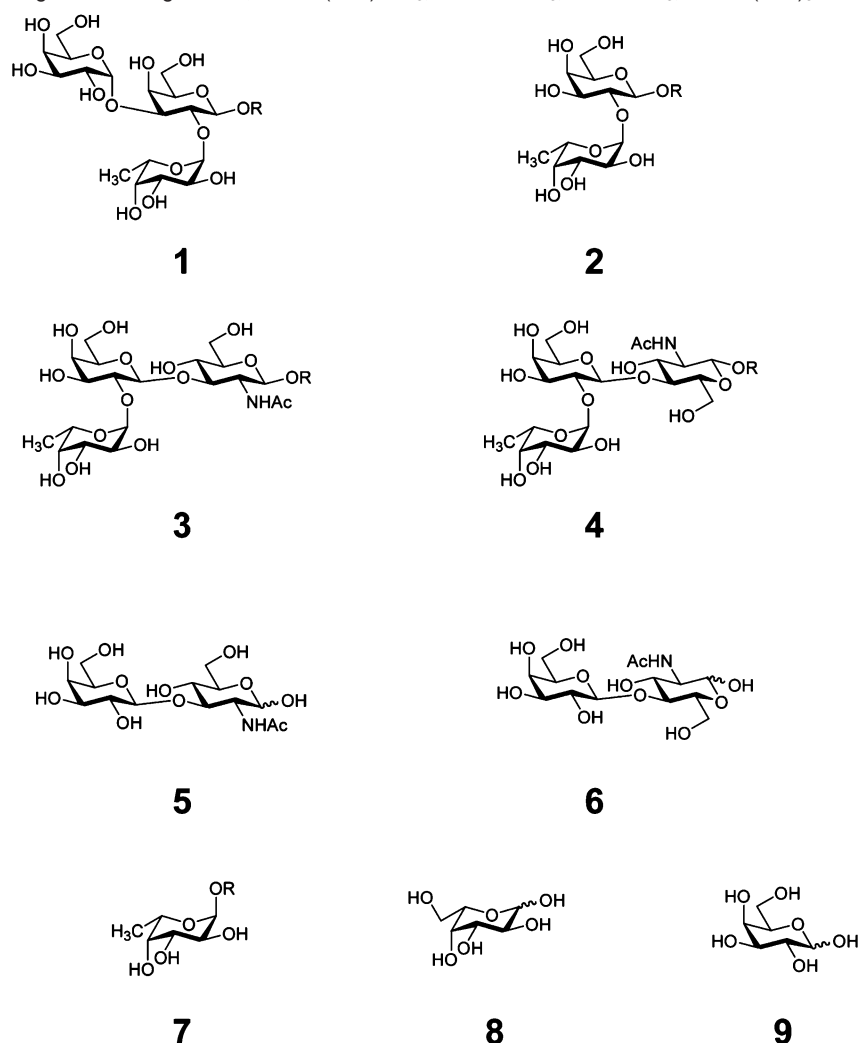
being the transverse relaxation rate, x being the offset from on-resonance, and a being the center of the Lorenz line. Error estimation was performed using a Monte Carlo-based procedure. The values generated by the nonlinear least-squares fitting were regarded as "true" values. A Gaussian distribution was assigned to each data point with the difference between the experimental and the "true" value being the standard deviation σ. Next, for each data point a random number was generated from the corresponding Gaussian distribution to produce an artificial set of data. A nonlinear least-squares fitting was performed for this new artificial set of data. This process was repeated 500 times (500 MC steps). The standard deviation of the line width is calculated from the individual line widths resulting from each Monte Carlo step. The different gray shades seen in Figure 1 result from the overlay of curves resulting from the individual nonlinear least-squares fits.

Results and Discussion

As most members of the *Caliciviridae* are non-cultivatable, we have used virus-like particles (VLPs) that are morphologically and antigenically indistinguishable from native virions.[21–23]

RHDV VLPs dissolved in PBS buffer and in the presence of a 25−50-fold molar excess of carbohydrate ligands were subjected to STD NMR experiments using standard pulse sequences as described before.[4,24–27] In short, one saturates the protons of the viral capsid with an appropriate radio frequency field. The irradiation frequency of this so-called on-resonance experiment is chosen such that the proton resonances of the carbohydrate ligands are not affected. If a carbohydrate ligand binds to the viral surface, saturation is transferred from the protons in the binding pocket of the virus on to protons of the ligand. The amount of this saturation transfer is determined by the dissociation rate k_{off} and the dissociation constant K_D of the corresponding complex. Non-binding molecules are not affected. Thus, besides a mere discrimination between binding and non-binding ligands, the binding pocket of the virus also leaves its structural imprint on the ligand, and ligand protons that are in close contact with protons in the viral binding pocket will receive more saturation than those located further away. This allows a fast analysis of the binding epitopes of a variety of ligands. To make these imprints visible, a second so-called off-resonance experi-

(21) Plana-Duran, J.; Bastons, M.; Rodriguez, M. J.; Climent, I.; Cortes, E.; Vela, C.; Casal, I. *Arch. Virol.* **1996**, *141*, 1423−36.
(22) Marin, M. S.; Martin Alonso, J. M.; Perez Ordoyo Garcia, L. I.; Boga, J. A.; Arguello-Villares, J. L.; Casais, R.; Venugopal, K.; Jiang, W.; Gould, E. A.; Parra, F. *Virus Res.* **1995**, *39*, 119−28.
(23) Laurent, S.; Vautherot, J. F.; Madelaine, M. F.; Le Gall, G.; Rasschaert, D. *J. Virol.* **1994**, *68*, 6794−8.

(24) Mayer, M.; Meyer, B. *J. Am. Chem. Soc.* **2001**, *123*, 6108−17.
(25) Mayer, M.; Meyer, B. *Angew. Chem., Int. Ed.* **1999**, *38*, 1784−1788.
(26) Moser, R.; Snyers, L.; Wruss, J.; Angulo, J.; Peters, H.; Peters, T.; Blaas, D. *Virology* **2005**, *338*, 259−69.
(27) Meyer, B.; Peters, T. *Angew. Chem., Int. Ed.* **2003**, *42*, 864−890.
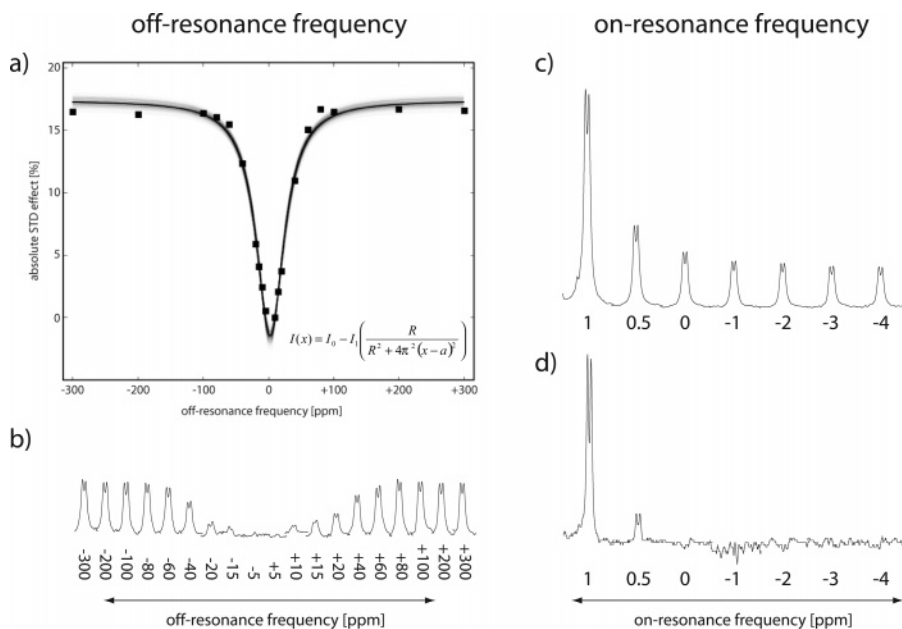
Figure 1. Saturation transfer profiles for RHDV VLPs. (a) STD experiments were acquired with variable off-resonance frequencies varying from −300 to +300 ppm, and one constant on-resonance frequency of −4 ppm. Three proton signals of α-L-Fuc-OMe, H1, -OCH₃, and CH₃-6 (H6) were chosen to indirectly sample the overall line width of the RHDV VLP. These protons were chosen because their resonance signals are isolated and do not show strong couplings to other protons. In addition, they are characterized by rather different environments in the binding site. This is important because this line width analysis should be independent of the absolute size of the STD. The saturation profile resulting from saturation transfer to H6 is shown as a representative example (cf., Figure S7 of the Supporting Information for the other saturation profiles). The thick solid line represents the result of a nonlinear least-squares fit, whereas the thickness of the gray line reflects the result of a 500 step Monte Carlo simulation for error estimation. From this analysis, a "line width" of 26 kHz ± 1.5 kHz is obtained for the RHDV VLP. (b)−(d) Expansions of corresponding STD spectra showing the resonance signal of H6 of α-L-Fuc-*O*Me at 1.23 ppm. (b) Dependency of the STD signal intensity on the off-resonance frequency. (c) and (d) Dependency of the STD signal intensity on the on-resonance frequency. (c) STD signals in the presence of VLPs, and (d) in the absence of VLPs (direct irradiation). The data indicate that direct irradiation of H6 occurs at frequencies above 0.0 ppm. It is observed that the STD signal intensity is almost unaffected by variation of the on-resonance frequency in the range between 0 and −4 ppm (c). Similar results are observed for other ligand protons.

ment is performed, where the irradiation frequency is set at a value outside of the range of resonance frequencies of any of the protons of the virus or the ligand. The on-resonance experiment is subtracted from this off-resonance experiment to only yield ligand signals that have experienced saturation transfer. Quantification of the effects is rather straightforward and directly yields the binding epitope of the ligand at atomic resolution.

STD NMR Experiments with VLPs Require a Modified Setup. In the present case, we had to slightly modify the conventional setup for STD NMR experiments. For viruses and virus-like particles, it can be expected that the corresponding protons display very large line widths. This raises the question of where to best place the on- and off-resonance frequencies. It turns out that the on-resonance frequency can be set at rather low values of, for example, −4 ppm (as it was used throughout the experiments described in the present study). Even at this frequency, a very efficient saturation of the VLPs was observed. This is very convenient as it safely avoids any direct irradiation of ligand signals. The setting of the off-resonance frequency is more critical because one has to make sure that no "residual" saturation of the viral capsid protons occurs during the off-resonance experiment that would lead to an attenuation of intensities in the difference spectra.

To identify a "safe" off-resonance frequency, we subjected α-L-Fuc-OMe to STD NMR experiments in the presence of RHDV at varying off-resonance frequencies (Figure 1).

α-L-Fuc-OMe was chosen for these experiments because it yielded STD NMR spectra with excellent signal-to-noise ratios

(see below). The off-resonance frequencies were varied over a range of ±300 ppm to identify the best conditions for such experiments. Excitation profiles were recorded for H1, CH₃-6, and OCH₃ of α-L-Fuc-OMe. It is observed that the signal envelope of the VLP is rather broad, and even at off-resonance frequencies of about ±50 ppm there are still significant on-resonance contributions that lead to a decrease of observed STD signals. Presumably, this is also the case for other viruses and VLPs and should be kept in mind when optimizing the experimental setup for such systems. Interestingly, the saturation profiles can be fitted to Lorenzian lines, supporting the assumption that it is indeed the signal envelope of the VLP that is reflected by the excitation profile. Nonlinear least-squares curve fitting yields a "line width" of the VLPs of ca. 26 kHz. Therefore, in our experiments, we have chosen an off-resonance frequency of 300 ppm so as not to produce artifacts.

For the quantitative analyses of STD effects observed in such high molecular weight systems, one has to exercise some degree of caution in using the traditional relaxation theory in non-viscous liquids based on "Motional Narrowing Approximation"[28] because for the large virus particle its long rotational correlation time can no longer be negligibly short as compared to its own relaxation times. Therefore, the following analysis will be qualitative and focus on a comparison between different binding epitopes of ligands and biological implications from this, rather than attempting to yield structural details for the

(28) Slichter, C. P. *Principles of Magnetic Resonance*, 3rd ed.; Springer-Verlag: Berlin, Heidelberg, New York, Barcelona, Budapest, Hongkong, London, Milan, Paris, Santa Clara, Singapore, Tokyo, 1996; Vol. 1.
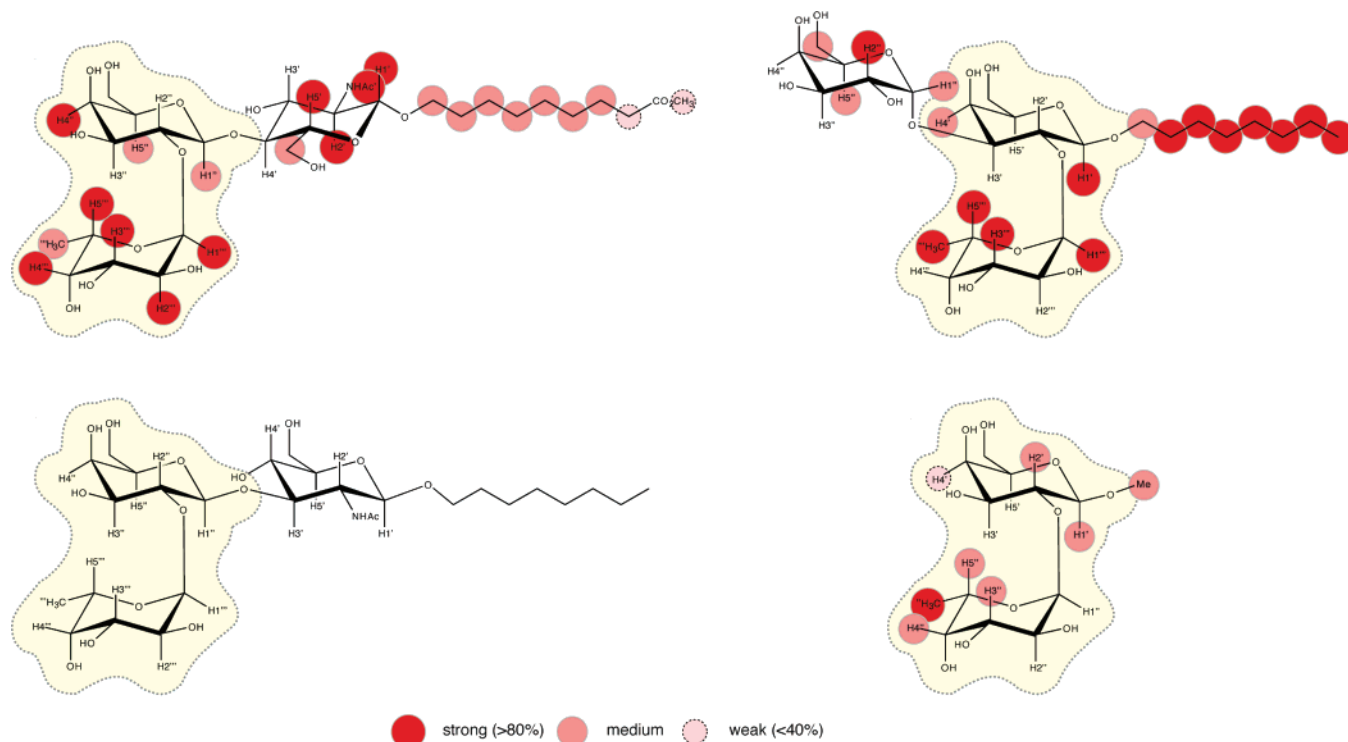
Figure 2. Binding epitopes of the oligosaccharide receptor fragments used in this study. Pale yellow background color highlights the H-disaccharide fragment common to all saccharides investigated. Colored circles reflect the relative size of the STD effects. For each molecule, the largest absolute STD effect has been scaled to 100%. The absence of a circle does not imply the absence of saturation transfer to this proton (saturation transfer has been observed for all protons) but rather indicates that the corresponding resonances are not fully resolved, and therefore STD effects cannot be determined unambiguously. All epitopes are based on the analysis of the initial slopes of the STD curves (cf., Figure S3).

VLP−ligand complexes using a motional narrowing-based relaxation theory.

STD NMR Experiments Yield Binding Epitopes and Minimal Structural Requirements for Specific Molecular Recognition of Blood Group Antigens. For the analysis of binding epitopes, we have employed the measurement of initial slopes of saturation transfer effects to minimize the effects of spin diffusion, and to obtain a better reproducibility of the data. This procedure automatically yields an experimental error (cf., Supporting Information). The resulting binding epitope for the H-type II trisaccharide (Scheme 1) is shown in Figure 2, and a corresponding STD NMR spectrum is shown in Figure 3.

From Figure 2, it is obvious that the *N*-acetyl-D-glucosamine (D-GlcNAc) residue and the L-fucose (L-Fuc) residue receive the largest fraction of saturation transfer. Apparently, the octyl spacer is only in rather loose contact with the viral surface.

In contrast to the H-type I and H-type II trisaccharides, the B-trisaccharide and the H-disaccharide (Schemes 1 and 2) lack the glycosidic linkage that discriminates type I and type II structures. Both the H-disaccharide and the B-trisaccharide show significant STD effects that reflect binding to RHDV (Figure 3). Therefore, elongation with a galactose residue at the non-reducing end of the blood group antigen apparently does not interfere with specific recognition of the receptor,[10] and as observed for the H-type II trisaccharide the fucose residue is receiving the largest fraction of saturation transfer. It is well known that superposition of type I and type II disaccharides such that the non-reducing pyranose units match places the

N-acetyl and the exo-cyclic hydroxy methyl groups of the reducing GlcNAc residue into opposite directions (cf., Figure 1S of the Supporting Information). Therefore, the discrimination of the type I and type II structures by RHDV is most likely due to this subtle structural difference.

To further illustrate the dependency of the molecular recognition process on the type of glycosidic linkage that discriminates type I from type II antigens, we also subjected the type I and type II disaccharides (Schemes 1 and 2) to STD NMR experiments in the presence of RHDV VLPs (cf., Supporting Information, Figure S2). The spectra show almost no STD responses, indicating very weak binding.

To identify minimal structural requirements for binding of HBGAs to RHDV, we subjected monosaccharide fragments and selected low molecular weight compounds to STD NMR experiments in the presence of RHDV VLPs. We selected β-D-Gal-OMe and α-L-Fuc-OMe because both monosaccharides are fragments of HBGAs. D-Glucose was chosen as a negative control. The experiments (Figure 3) demonstrate that RHDV VLPs very selectively recognize α-L-Fuc-OMe, because only for this monosaccharide STD effects were observed. The STD effects for α-L-Fuc-OMe were large, and the resulting binding epitope is presented with the Supporting Information (Figure S4).

Ethanol, methanol, and L-Trp were also subjected to STD NMR experiments. Small STD effects that were observed for ethanol and methanol are the result of loose associations of these molecules with, for example, hydrophilic side chains on the surface of the VLPs just as bound water also gives an STD response. For L-Trp, significant STD signals were
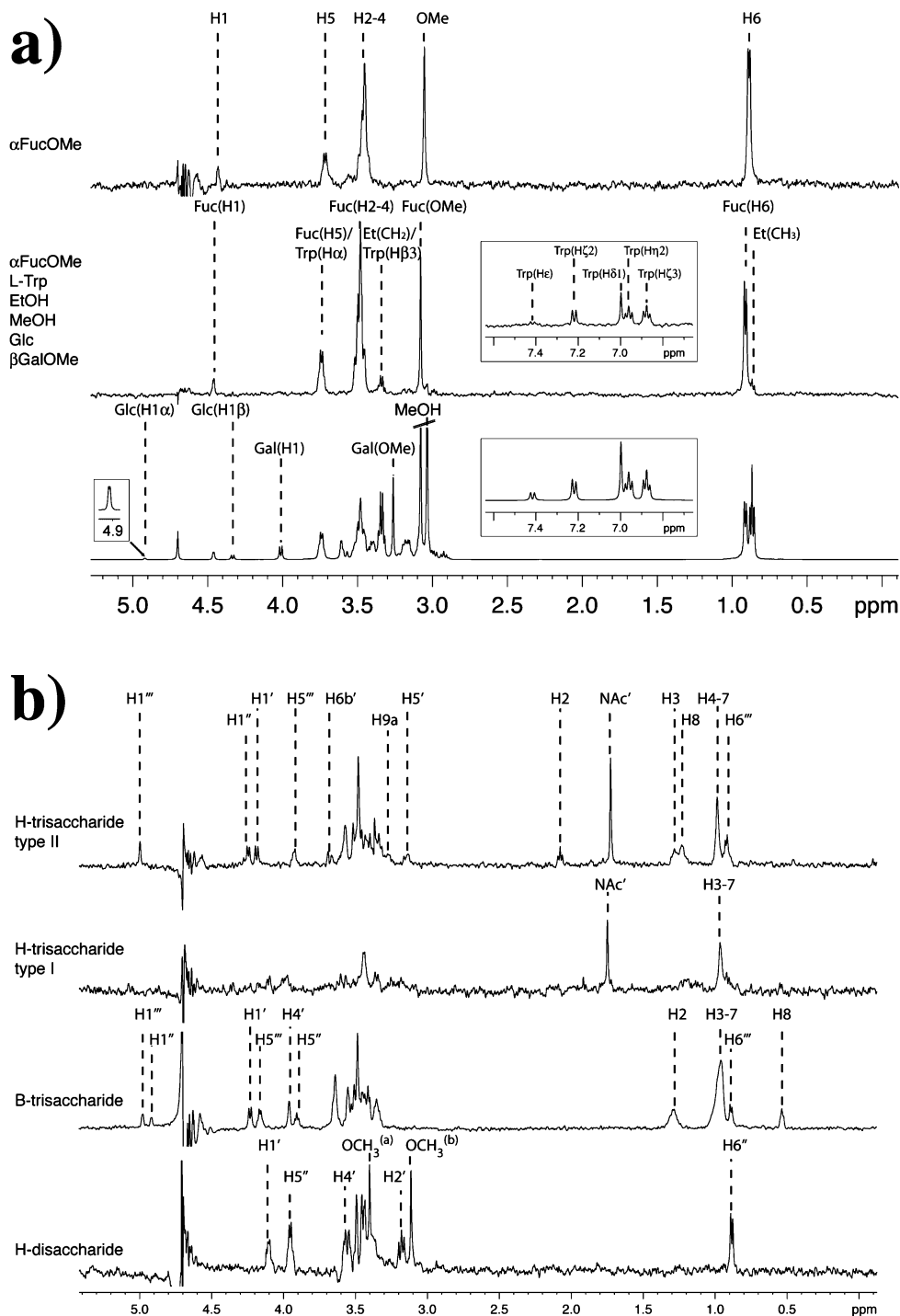
Figure 3. STD NMR spectra of synthetic carbohydrates and a compound mixture in the presence of RHDV VLPs. (a) From top to bottom, STD spectra of α-L-Fuc-OMe, a compound mixture comprising L-tryptophan, glucose, β-D-GalOMe, ethanol, and methanol, and a reference spectrum of the mixture are shown. Dashed lines highlight proton resonance assignments. Resonances of aromatic protons of L-tryptophan are shown in insets. STD effects from L-tryptophan as well as from ethanol and methanol result from unspecific binding. (b) From top to bottom, STD NMR spectra of H-trisaccharide type II (**4**), H-trisaccharide type I (**3**), B-trisaccharide (**1**), and the H-disaccharide (**2**) are shown. All spectra were recorded in the presence of $10-20 \mu$M RHDV VLP binding sites and up to 1 mM of ligand. The on-resonance frequency was set at -4 ppm, and off-resonance saturation was at $+300$ ppm. The spectra shown were recorded with 0.5 s saturation time and 3-9-19 WATERGATE for water suppression.

observed for the aromatic side chain, also indicating binding to RHDV. To test whether L-Trp occupies the same binding pocket as the blood group antigens or L-fucose competition, STD NMR experiments with α-L-Fuc-OMe were performed (cf., Supporting Information). The experiments unambiguously show that the STD effects of L-Trp are unaffected by the

presence of α-L-Fuc-OMe, demonstrating that L-Trp binds to another site(s).

A comparison of the binding epitope of the monosaccharide α-L-Fuc-OMe to the one of α-L-Fuc as part of the H-type II trisaccharide, or the B-trisaccharide, or the H-disaccharide shows differences suggesting slightly different binding modes of the

Table 1. Overview of HBGA Binding to RHDV VLPs

name	structure	binding to RHDV VLPs[a]
di- and trisaccharides:		
H-antigen disaccharide	α-L-Fuc-(1,2)-β-D-Gal-(1,O)-(CH$_2$)$_7$-CH$_3$	++
H-antigen type I	α-L-Fuc-(1,2)-β-D-Gal-(1,3)-β-D-GlcNAc-(1,O)-(CH$_2$)$_7$-CH$_3$	−
H-antigen type II	α-L-Fuc-(1,2)-β-D-Gal-(1,4)-β-D-GlcNAc-(1,9)-(CH$_2$)$_8$-COOCH$_3$	++
B-antigen trisaccharide	α-L-Fuc-(1,2)-(α-D-Gal-(1,3))-β-D-Gal-(1,O)-(CH$_2$)$_7$-CH$_3$	++
disaccharide type I	β-D-Gal-(1,3)-(α/β)-D-GlcNAc	−
disaccharide type II	β-D-Gal-(1,4)-(α/β)-D-GlcNAc	+
monosaccharides:		
	α-L-Fuc-O-CH$_3$	++
	α/β-D-Fuc	−
	β-D-Gal-O-CH$_3$	−
	α/β-L-Gal	++
other ligands:		
L-Trp[b]	L-tryptophan	++
ethanol[b]	CH$_2$CH$_3$OH	+
methanol[b]	CH$_3$OH	+

[a] ++ indicate strong STD effects, + indicate weak STD effects, and − indicate no STD observed. [b] Do not bind into the carbohydrate binding site.

fucose residue in the different cases. Although the H-type I trisaccharide contains a fucose that constitutes the minimal binding requirement, in this case hardly any STD signals are observed. Therefore, unfavorable steric contacts with the capsid binding pocket must be significant (cf., Supporting Information, Figure S1).

To further assess the degree of specificity of the recognition reaction, we finally compared the chemically closely related monosaccharides L-fucose, D-fucose, L-galactose, and D-galactose. D-Fucose as well as D-galactose did not yield any STD signals, whereas L-fucose and L-galactose yielded substantial STD effects (cf., Supporting Information). This observation emphasizes the high selectivity with which RHDV binds to its receptor.

Conclusions

To summarize, our studies yield a comprehensive binding topology of the blood group antigen receptor for RHDV at atomic resolution (Figure 2 and Table 1). We have demonstrated that L-fucose and L-galactose represent minimal structural requirements for specific molecular recognition by RHDV. This information is essential for the design of low molecular weight, high affinity binders to RHDV that finally could be turned into RHDV entry inhibitors. It is envisioned that the strategy described in this Article is suitable for the design of entry inhibitors of non-enveloped viruses in general.

Supporting Information Available: Figure S1: Stick representations of β-D-Gal-(1,3)-β-D-GlcNAc (type I disaccharide **5**) and β-D-Gal-(1,4)-β-D-GlcNAc (type II disaccharide **6**). Figure S2: STD NMR spectra of type I and II disaccharides in the presence of RHDV VLPs. Figure S3: Initial STD build-up curves for type II trisaccharide **4**. Figure S4: Binding epitope of α-L-Fuc-OMe **7**. Figure S5: Expansion of the aromatic region of STD NMR and reference NMR spectra of L-Trp. Figure S6: STD and reference NMR spectra of L-galactose and D-fucose in the presence of H-antigen type I trisaccharide **3**. Figure S7: Saturation profiles. Table S1: ^{1}H and ^{13}C NMR chemical shifts, ^{1}H T_1 values. Table S2: Initial slopes from STD build-up curves for epitope analysis. This material is available free of charge via the Internet at http://pubs.acs.org.

JA710854R